IEEE Access
Multidisciplinary | Rapid Review | Open Access Journal

Received February 25, 2020, accepted March 5, 2020, date of publication March 25, 2020, date of current version April 24, 2020.

Digital Object Identifier 10.1109/ACCESS.2020.2983155

Morphological, Texture, and Color Feature Analysis for Erythrocyte Classification in Thalassemia Cases

DYAH ARUMING TYAS[1], SRI HARTATI[1], AGUS HARJOKO[1], AND TRI RATNANINGSIH[2]

[1]Department of Computer Science and Electronics, Universitas Gadjah Mada (UGM), Yogyakarta 55281, Indonesia
[2]Department of Clinical Pathology, Faculty of Medicine, Public Health and Nursing, Universitas Gadjah Mada (UGM), Yogyakarta 55281, Indonesia

Corresponding author: Agus Harjoko (aharjoko@ugm.ac.id)

This work was supported by The Research Directorate of Universitas Gadjah Mada, Rekognisi Tugas Akhir (RTA) Scheme and Directorate General of Higher Education, Ministry of Research and Education, Indonesia, (PMDSU Scheme), under Grant 2019.

ABSTRACT Abnormal erythrocytes have diverse shapes. The appearance of specific erythrocyte shapes in a person's blood can indicate certain diseases, including thalassemia. We used thalassemia peripheral blood smear images and applied a segmentation process to produce single erythrocyte sub-images. Each erythrocyte has a unique shape. The selection of appropriate features to represent erythrocytes is critical for classification accuracy. We used morphological features such as moment invariants, geometry parameters of the cell and central pallor, and distance angle signature (DAS) morphological features of the cell and central pallor. We combined morphological features with texture and color features to increase the accuracy of erythrocyte classification. In this study, the multi-layer perceptron is used to classify nine shapes of erythrocytes present in thalassemia cases. The experimental results of 7108 erythrocytes indicated an accuracy of 98.11% based on the combination of features. The experimental results also show that the combination of features we proposed produced higher classification accuracy than previous work, which yielded an accuracy of 93.77%.

INDEX TERMS Classification, distance angle signature, erythrocytes, morphological feature, thalassemia.

I. INTRODUCTION

The abnormal form of erythrocytes can indicate certain diseases, including thalassemia. Thalassemia is one of the most prevalent diseases in the world. Akay *et al.* investigated the social, economic, and geographical dynamics of the spread of β -thalassemia [1]. Thalassemia causes erythrocytes to be destroyed rapidly, and patients must have regular blood transfusions to maintain red blood cells. However, regular blood transfusions cause iron overload that can lead to complications such as heart failure, diabetes, kidney disorders, and osteoporosis. Iron overload measurement has become a separate topic to be investigated [2], [3].

Based on the 2015 ICSH [4] erythrocyte abnormalities can be determined from the morphology, size, and color of erythrocytes. In thalassemia cases, erythrocytes will appear paler and microcytic (smaller in size) compared to normal erythrocytes. Erythrocytes with diverse morphology will also be found in the blood of thalassemia patients, in target cells, teardrop cells, ellipse cells, hypochromic cells, and other cells. In the thalassemia screening process, a laboratory assistant must observe and count the number of abnormal red blood cells from visual microscopic observations in peripheral blood smear preparations to assess erythrocytes. The result of a manual review of erythrocytes is a report of clinically meaningful cells requiring expertise and experience from laboratory staff [4].

Studies involving digital image processing technology and machine learning (ML) in the medical field are increasing. In studies related to blood cells, researchers use a blood smear image to be processed. The research usually aims to count and recognize blood cells to identify diseases or abnormalities. In 2014, Tomari *et al.* [5] classified red blood cells (RBC) in blood smear images into normal and abnormal types. In 2015, Sarrafzadeh *et al.* [6] conducted a study on segmentation and RBC count using the circlet transform method proposed by Chauris *et al.* [7]. Also in 2015, research on RBC cluster

The associate editor coordinating the review of this manuscript and approving it for publication was Donato Impedovo.

separation in sickle cell disease was published by González-Hidalgo [8].

In 2017, Elsalamony [9] introduced an algorithm for detecting anemia cells, such as sickle and elliptical cells, based on geometrical shape signature using neural networks. The study classified only elliptical cells and sickle cells. In 2018, Hartati *et al.* [10] assessed the performance of SVM and ANFIS for Classification of Malaria Parasite and Its Life-Cycle-Stages in Blood Smear. Setiawan *et al.* classify cell types in Acute Myeloid Leukemia (AML) of M4, M5, and M7 subtypes with a support vector machine classifier [11]. Research on the classification of malignant lymphoid cells and blast cells using SVM has been reported by Rodellar *et al.* [12]. The classification of five types of white blood cells using neural networks was conducted by Othman *et al.* [13]. Safuan *et al.* investigated white blood cell (WBC) segmentation using various color segmentation methods [14].

The features used in the study of blood cell classification are varied. Careful selection of features must be conducted to obtain accurate classification. Some features, such as geometry, color, shape, and texture are often used. Determination of features that represent erythrocytes for classification is important because the types of abnormal erythrocytes are diverse. This study aims to classify nine types of erythrocytes that often appear in thalassemia cases using the combination of morphological features, texture features and color features. The main contribution of this paper is to identify features that can be used to distinguish nine types of erythrocytes.

II. RELATED WORKS

Several studies have proposed methods for classifying red blood cells using various features. This section will describe several types of features used in red blood cell classification.

The combination of geometrical features, texture features, and shape features was chosen by Tyagi *et al.* [15] for detecting abnormal erythrocytes in cases of iron deficiency anemia using artificial neural networks. Feature extraction produced 34 features, which are all directly used in the classification process. The average classification accuracy was 77.75% for five types of erythrocytes (healthy cells, elliptocyte, dacrocyte/teardrop, degmacyte, and schistocytes). Geometry features were used in research by Dalvi and Vernekar [16]. Thirteen geometrical features were used in the classification of five types of erythrocytes (elliptocyte, echinocyte, teardrop, macrocyte, and healthy cells). The results of classification using the artificial neural network (ANN) algorithm and the Decision Tree Classifier (DTC) were compared, and it was found that ANN produced better accuracy than DTC, reaching 90.54%.

A combination of shape, geometry, and color features based on statistical analysis was used by Abood *et al.* (2017) [17] to classify blood cells into normal and abnormal classes. The extracted features were mean, standard deviation, variance, roundness, skewness, and kurtosis. Classification using the Fuzzy logic algorithm reached 98% accuracy. Research on the morphological features of erythrocytes in iron deficiency anemia (IDA) and thalassemia was conducted by Ahmad *et al.* [18]. They proposed 24 and 31 features, respectively, consisting of Hue's moment, Zernike moment, Fourier descriptor, and geometry features to classify nine types of erythrocytes. In the study, the best subsets of 31 features provide 83.5% accuracy, 83.5% sensitivity, and 83.3% positive predictive value, via logistic regression compared to other classifiers. Another study proposed moment invariants and geometric parameters such as area, perimeter, major axis, minor axis, texture features (contrast, correlation, homogeneity, and energy derived from the GLCM method), and color (mean, standard deviation, kurtosis, and skewness of RGB and grayscale images) to classify red blood cells [19].

Signature-based features can also be used in classification. In the process of detecting erythrocyte abnormalities in sickle cell anemia and thalassemia, Sharma *et al.* [20] used a combination of the variance of radial signature features, metric values (the level of object roundness), and aspect ratios (ratio of the major axis and minor axis). Radial signature is a representation of a 2-D object shape into a 1-D function from a radial distance (r) and an angle. The classification stage used a K-Nearest Neighbor (KNN) algorithm, which produced an accuracy of 80.6% and a sensitivity of 87.6%. Elsalamony [9] used the value of AVD (absolute deviation from the center point of the object to all points on the edge of the object) and DIF (the difference between the input absolute deviation with the stored absolute value of the cell's absolute deviation). The AVD and DIF obtained from the shape signature were combined with perimeter, area, eccentricity, convex area, ratio, and solidity. Two ANNs were used in the classification stage. The first ANN was used to distinguish sickle cells from normal cells and other abnormal cells, and the second ANN was used to distinguish elliptocytosis cells from normal cells or other abnormal cells. Elsalamony's method can classify oval cells and sickle cells very well but has not classified circular blood cells according to their type.

Currently, the deep learning method is popular for classification in many domains. Tyas *et al.* have reported the comparison result of erythrocyte classification using a backpropagation neural network and convolutional neural network (CNN). The result showed that the backpropagation neural network yields higher accuracy than CNN [19]. The comparison result of SVM and AlexNet in classifying color images of erythrocytes was reported by Aliyu *et al.* The result showed that SVM yields higher accuracy than AlexNet [21]. In leukocyte classification, Qin *et al.* presented a fine-grinned leukocyte classification method using a deep residual neural network [22]. They classified 40 leukocyte categories from almost one hundred thousand leukocyte images and reached an average accuracy of 76.84%.

III. THE PROPOSED METHOD

This section explains our method for classifying nine types of erythrocytes that often appear in thalassemia cases. The method consists of image acquisition, segmentation, feature

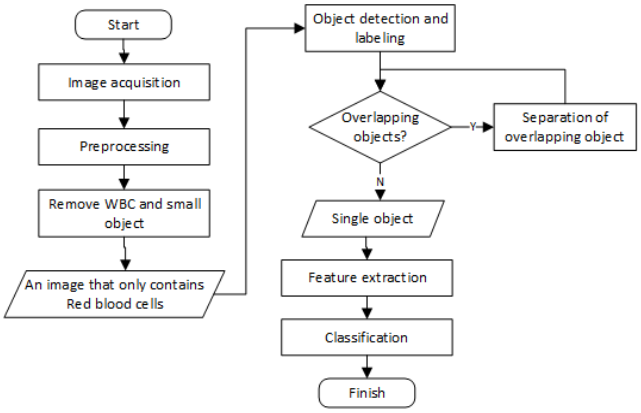

FIGURE 1. Stages of proposed method.

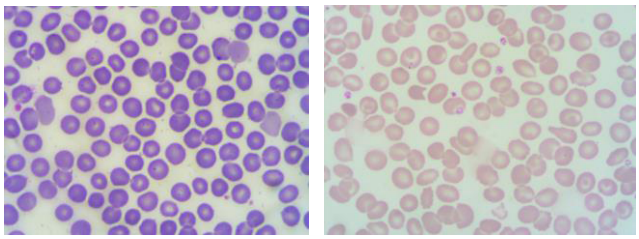

FIGURE 2. Peripheral blood smear sample image of (a) healthy individuals and (b) minor thalassemia individuals.

extraction, and classification. The stages of the proposed method shows in Fig. 1.

A. IMAGE ACQUISITION AND PREPROCESSING

Image acquisition is the process of retrieving microscopic image data from peripheral blood smears through a microscope using a camera specifically for the microscope (Optilab). In this study, thalassemia peripheral blood smears and healthy peripheral blood smears were obtained from the Clinical Pathology Laboratory of the Faculty of Medicine, Public Health and Nursing, Universitas Gadjah Mada, Indonesia. Fig. 2 shows sample images of (a) a healthy peripheral blood smear and (b) a minor thalassemia peripheral blood smear. Laboratory assistants helped obtain ideal erythrocyte images. After image acquisition, the image is resized from 4100 × 3075 pixels to 800 × 600 pixels to reduce the computing load in the next stage. We extracted the green color component (green channel) of the RGB image and used it in the next process. We chose the green channel because it is not affected by variations in color and brightness. Fig. 3 and Fig. 4 shown the histogram of each channel of the RGBm YCbCr, and HSV. Top row shown RGB image, red channel histogram, green channel histogram, blue channel histogram. Middle row shown YCbCr image of the RGB image, Y channel histogram, Cb channel histogram, Cr channel histogram. Bottom row shown HSV image of the RGB image, hue channel histogram, saturation channel histogram, value channel histogram. As shown in Fig. 3 and Fig. 4, green channel histograms on the RGB color space consistently show a separate object and background. This is indicated by the presence of two peaks on the histogram. Median filtering was performed to reduce noise in the image.

TABLE 1. Features obtained from feature extraction.

Type of features	Features	No. of features
Texture	GLCM set of features	20
Color	Color moment	4
Shape	Geometry parameters of cell	7
	Geometry parameters of central pallor	8
	Moment invariants (Hue's moment) of cell	7
	DAS morphology of cell	9
	DAS morphology of central pallor	9
Total of features		64

B. SEGMENTATION

The segmentation process produces sub-images that contain only red blood cells, using binarization, morphological operations, hole filling operations, and watershed distance transform. After we perform object detection and labeling, we define a threshold area on each detected object to split single cells and overlap cells, assuming the overlap cells have an area larger than a single cell. Overlapping objects are separated using the circle hough transform. Segmentation produces a sub-image of a single blood cell, as shown in Fig. 5.

C. FEATURE EXTRACTION

Features that can be extracted from the erythrocytes are shape, texture, and color. We used moment invariants, geometric parameters, and distance angle signature (DAS) as shape feature extraction methods, and gray level co-occurrence matrices (GLCM) as the texture feature extraction method. We used mean, standard deviation, skewness, and kurtosis of the green channel pixel values as color features. Extracted features are shown in Table 1.

1) TEXTURE FEATURE EXTRACTION USING GRAY LEVEL CO-OCCURRENCE MATRICES (GLCM)

GLCM are a second-order texture calculation. First-order texture measurements use statistical calculations based on the original pixel value of the image, such as variance, and do not consider the relationship of neighboring pixels. In second-order texture measurements, the relationship between two-pixel pairs of the image is used in the calculation. In GLCM [23], contrast, correlation, energy, and homogeneity values are obtained at angles of 0°, 45°, 90°, and 135°. The mean values of each feature are calculated, for a total of 20 feature values. GLCM feature values can be obtained from (1) − (4) [23].

$$Contrast = \sum_{n=0}^{Ng-1} n^2 \left\{ \sum_{i=1}^{Ng} \sum_{j=1}^{Ng} p(i,j) \right\}, \quad |i-j| = n \quad (1)$$

$$Correlation = \frac{\sum_i \sum_i (ij)p(i,j) - (\mu_i \mu_j)}{\sigma_i \sigma_j} \quad (2)$$

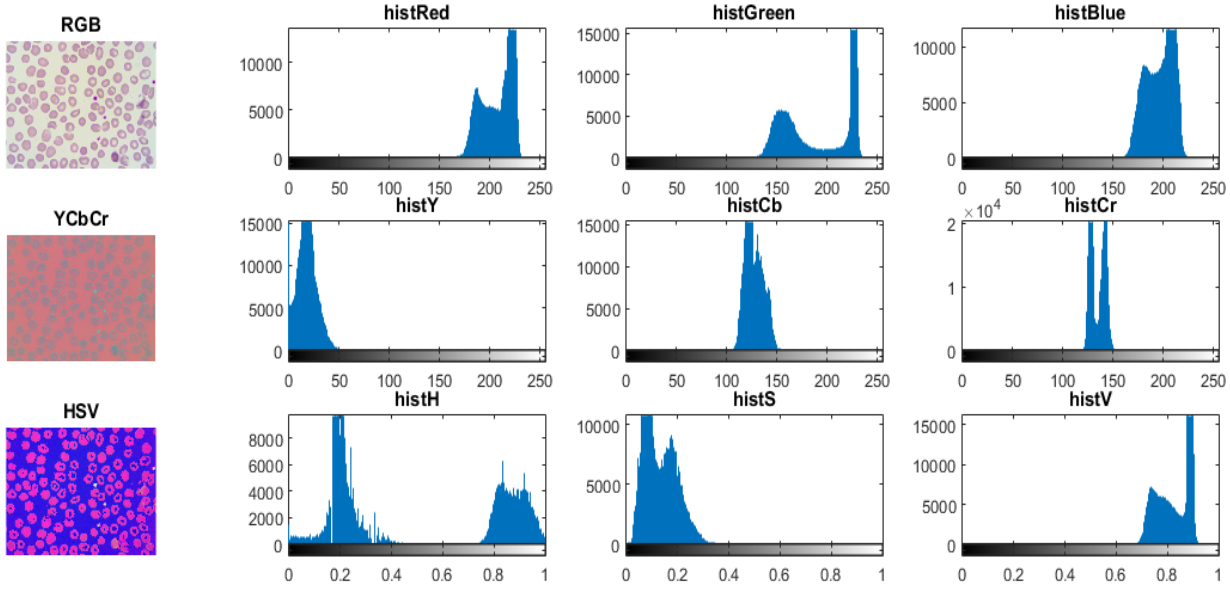

FIGURE 3. Histogram of each color channel of the RGB, YCbCr, and HSV color spaces in image sample 1. Top row: RGB image, red channel histogram, green channel histogram, blue channel histogram Middle row: YCbCr image of the RGB image, Y channel histogram, Cb channel histogram, Cr channel histogram Bottom row: HSV image of the RGB image, hue channel histogram, saturation channel histogram, value channel histogram.

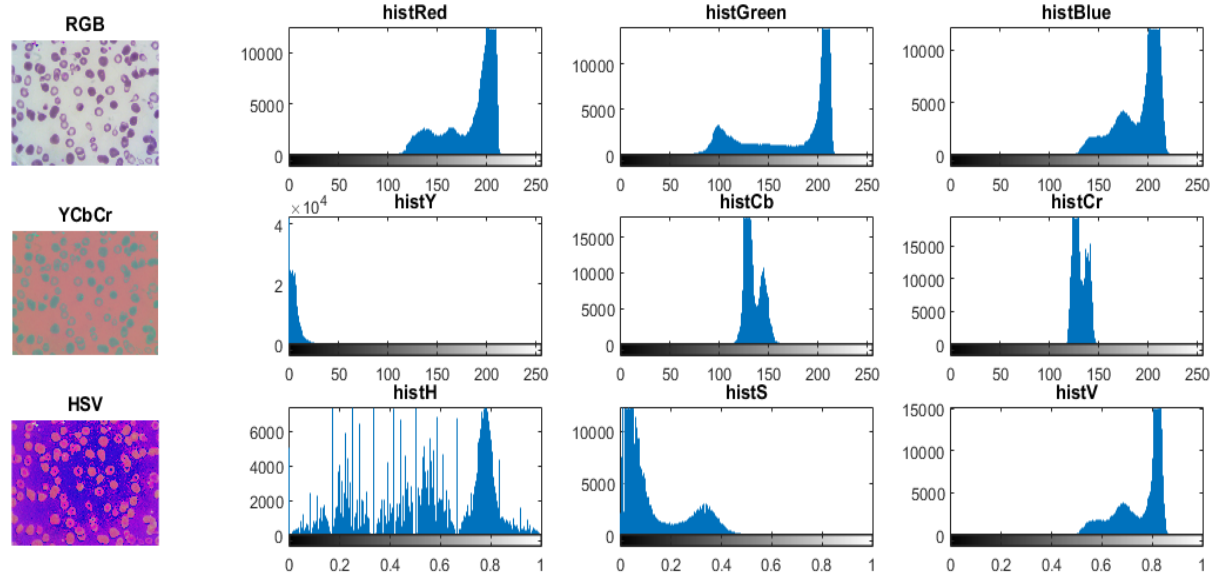

FIGURE 4. Histogram of each color channel of the RGB, YCbCr, and HSV color spaces in image sample 2. Top row: RGB image, red channel histogram, green channel histogram, blue channel histogram Middle row: YCbCr image of the RGB image, Y channel histogram, Cb channel histogram, Cr channel histogram Bottom row: HSV image of the RGB image, hue channel histogram, saturation channel histogram, value channel histogram.

$$Energy = \sum_{i,j} p(i,j)^2 \tag{3}$$

$$Homogeneity = \sum_{i} \sum_{j} \frac{1}{1+(i-j)^2} p(i,j) \tag{4}$$

where $p(i, j)$ is the distribution of joint probabilities of a pixel pair, one with gray level i and the other with gray level j. The symbol Ng is the number of gray levels used to build the GLCM. In this research, the gray level is 8. The symbols μ_i, μ_j, σ_i, σ_j are means and standard deviations of the marginal distributions associated with $p(i, j)$ and can be obtained from (5) - (8).

$$\mu_i = \sum_{i,j=0}^{Ng-1} i(P_{i,j}) \tag{5}$$

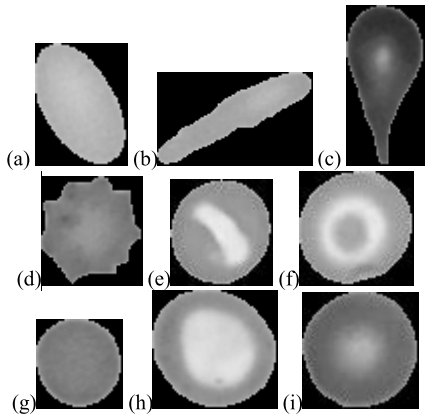

FIGURE 5. Sub-image of red blood cells: (a) Eliptocyte cell, (b) Pencil cell, (c) Teardrop cell, (d) Acanthocyte cell, (e) Stomatocyte cell, (f) Target cell, (g) Spherocyte cell, (h) Hypochromic cell, (i) Normal cell.

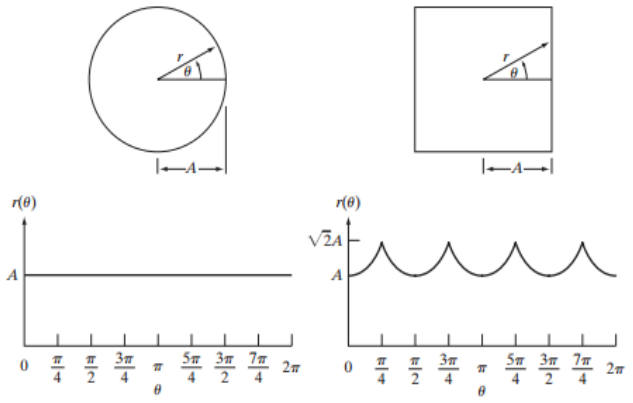

FIGURE 6. Illustration of distance versus angle signatures (DAS) in circular and square objects [26].

$$\mu_j = \sum_{i,j=0}^{Ng-1} j(P_{i,j}) \tag{6}$$

$$\sigma_i = \sum_{i,j=0}^{Ng-1} P_{i,j}(i - \mu_i) \tag{7}$$

$$\sigma_j = \sum_{i,j=0}^{Ng-1} P_{i,j}(j - \mu_i) \tag{8}$$

2) COLOR FEATURE EXTRACTION BASED ON THE COLOR MOMENT

Color moments are based on the assumption that color distribution in images can be interpreted as a probability distribution. If the color in the image follows a specific probability distribution, the moment of distribution can be used as a feature to identify images based on color. Color moment information consists of four sequences of moments. The first moment represents the mean color average (μ_c); the second moment is the standard deviation (σ_c), which expresses the distribution area; the third moment describes skewness (θ_c), which describes the size of the color asymmetry; and the fourth moment is kurtosis (γ_c), which shows the tapering or rounding of the distribution. The four color moments can be defined as (9) − (12), where the value of the color component c (grayscale) on the pixel color of the i^{th} row and the j^{th} column of the image is P_{ij}^c, and M and N are the width and height of the image, respectively, [24].

$$\mu_c = \frac{1}{MN} \sum_{i=1}^{M} \sum_{j=1}^{N} P_{ij}^c \tag{9}$$

$$\sigma_c = \sqrt{\frac{1}{MN} \left(\sum_{i=1}^{M} \sum_{j=1}^{N} \left(P_{ij}^c - \mu_c \right)^2 \right)} \tag{10}$$

$$\theta_c = \sqrt[3]{\frac{1}{MN} \left(\sum_{i=1}^{M} \sum_{j=1}^{N} \left(P_{ij}^c - \mu_c \right)^3 \right)} \tag{11}$$

$$\gamma_c = \sqrt[4]{\frac{1}{MN} \left(\sum_{i=1}^{M} \sum_{j=1}^{N} \left(P_{ij}^c - \mu_c \right)^4 \right)} \tag{12}$$

3) SHAPE FEATURE EXTRACTION USING MOMENT INVARIANTS AND GEOMETRY PARAMETERS

Feature extraction of shape using moment invariants produced seven moment invariant values that are not sensitive to translation, scale change, and rotation [25]. Geometric parameters are also used as shape features, including area, perimeter, major axis, minor axis, compactness, eccentricity, and solidity. A total of 14 feature values were extracted from the red blood cell using moment invariants and geometric parameters.

4) DISTANCE ANGLE SIGNATURE (DAS) MORPHOLOGICAL SHAPE FEATURE EXTRACTION

Signature features represent 1-D functions and can be extracted in various manners. A simple method is to plot the distance from the centroid to the boundary object as an angle function, as illustrated in Fig. 6. The concept of the signature is to reduce boundary representation into a 1-D function, which is more easily described than a 2-D boundary. Fig. 6 shows an illustration of distance versus angle signatures (DAS) in circular and square objects [26].

The signature of an object can be obtained by converting the initial image into a binary image to produce the object boundary. The distance of the centroid point of the object to the point on the boundary, r (in pixels), is calculated starting from $\theta = 1°$ to $\theta = 360°$ with angular shifts every 1°. After obtaining the distance r for each θ, the smallest value of r is found as the starting point to produce a signature. The starting point is used to overcome the rotation of the object. We can assume that each part of the image will produce a unique value. Therefore, we will find the starting point by using the

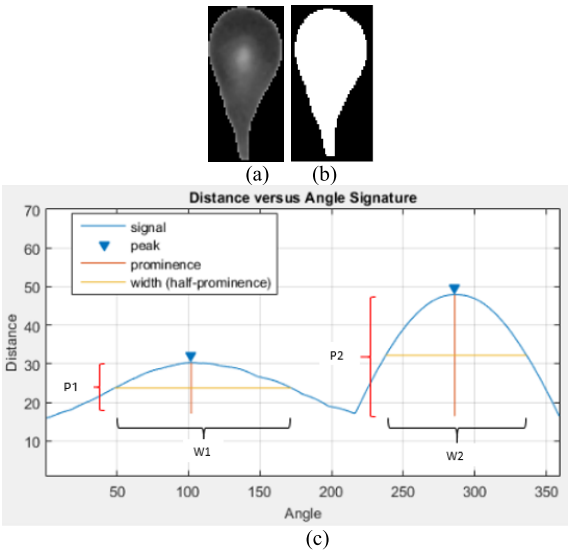

FIGURE 7. (a) Grayscale image of teardrop cell; (b) Binary image of teardrop cell; (c) Distance versus angle signature (DAS) graph of teardrop cell.

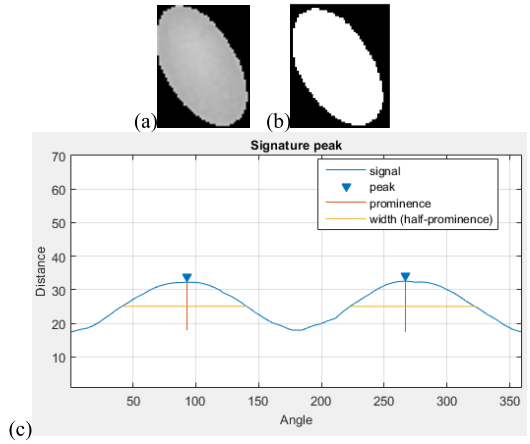

FIGURE 8. (a) Elliptocyte cell; (b) Binary image of elliptocyte cell; (c) Distance versus angle signature (DAS) graph of elliptocyte cell.

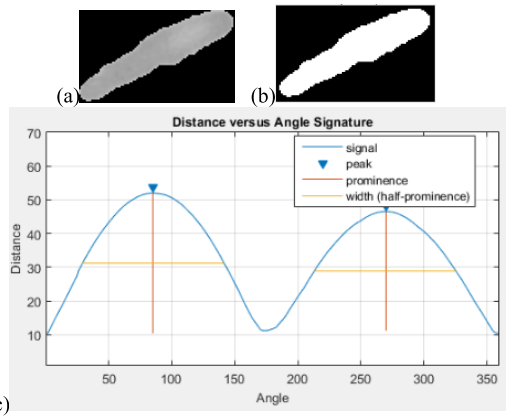

FIGURE 9. (a) Pencil cell; (b) Binary image of pencil cell; (c) Distance versus angle signature (DAS) graph of pencil cell.

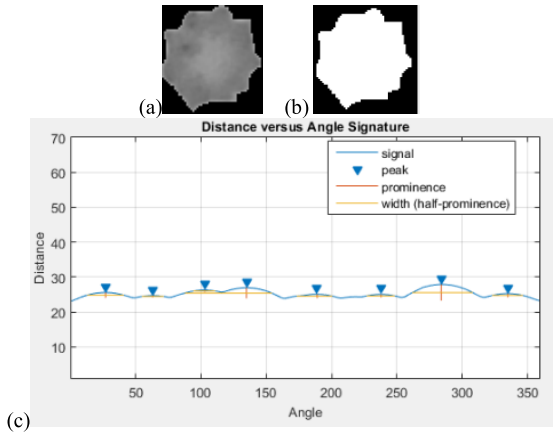

FIGURE 10. (a) Acanthocyte cell; (b) Binary image of acanthocyte cell; (c) Distance versus angle signature (DAS) graph of acanthocyte cell.

smallest value, regardless of image rotation. The final step is to plot the distance and angle on the Cartesian graph, known as the distance versus angle signature (DAS).

In this research, we propose shape features based on DAS graph morphology, namely prominence and width of the peak in the distance versus angle signature (DAS) graph. Each erythrocyte cell has a unique shape which produces a typical DAS graph. Figs. 7 - 13 show erythrocyte cells and corresponding DAS graphs. Fig. 7(c) shows a DAS graph of a teardrop cell that has two peaks with different heights and widths. We used a Matlab function, *findpeaks*(), to obtain the value of local maxima, prominence, and width. Peak prominence measures how prominent a peak is against another peak. Prominence is the minimum vertical distance that the signal has to travel on both sides before increasing to a higher peak or reaching the endpoint. The width of the peak is the distance between points on either side of the peak intersecting the signal at a certain height. In Fig. 7(c), the peak prominence is indicated by the red lines P1 and P2; the peak width is indicated by the orange lines W1 and W2.

The signature generated from a circular object is a straight line signature, as shown in Fig. 6. In this study, circular cell boundaries do not produce a straight line signature. As shown in Figs. 11 - 13, spherocytes, hypochromic cells, normal cells, and other circular cells do not always have perfect circular shapes. The resulting DAS graphs of circular cells have some very low peaks. The DAS graph of an acanthocyte cell has eight peaks, which represent the pointed parts of the cell body, as shown in Fig. 10. To meet the criteria for circular cells and acanthocyte cells in the DAS graphs, we use a peak height threshold value of 0.5. Processed peaks have a peak height greater than 0.5. This threshold aims to obtain the fewest number of peaks in the circular cell DAS graph and the most suitable number of peaks in the acanthocyte DAS graph. The threshold value is chosen based on observations of circular cell and acanthocyte signatures.

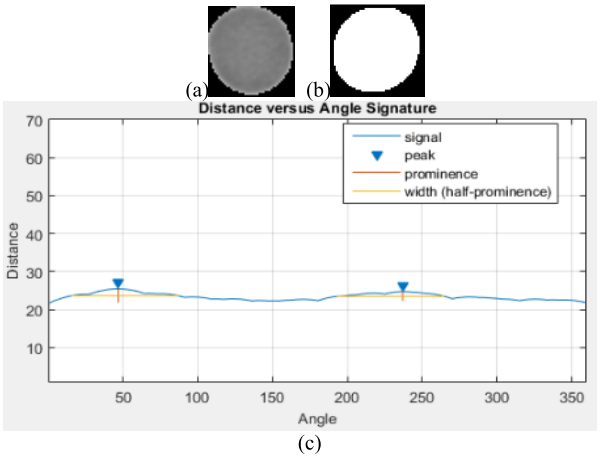

FIGURE 11. (a) Spherocyte cell; (b) Binary image of spherocyte cell; (c) Distance versus angle signature (DAS) graph of spherocyte cell.

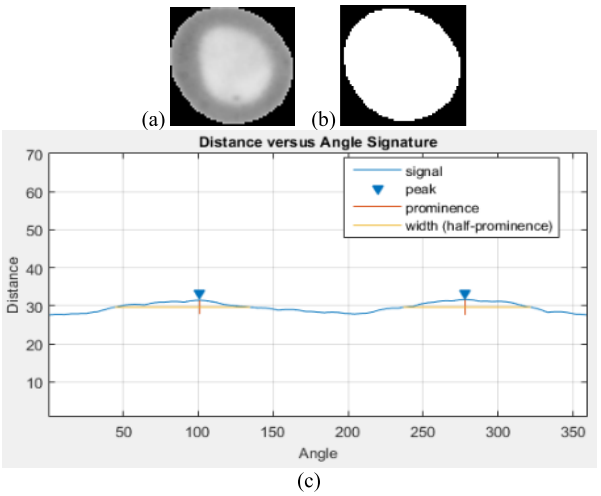

FIGURE 12. (a) Hypochromic cell; (b) Binary image of hypochromic cell; (c) Distance versus angle signature (DAS) graph of hypochromic cell.

In determining the peak width, the peak prominence value used as a reference is half of the peak prominence. As shown in Fig. 7(c), the peak width line is positioned at half of the peak prominence for each peak. In other words, the peak prominence line and the peak width line intersect at half of peak prominence. Figs. 8 - 13 show DAS graphs with the peaks marked with a blue triangle based on the specified threshold. Fig. 8(c) is a DAS from an elliptocyte cell that produces two peaks. Fig. 9(c) shows a DAS graph from a pencil cell that produces two peaks. Although the elliptocyte cell and pencil cell have the same number of peaks, we can see from Fig. 8(c) and Fig. 9(c) that the DAS graphs have different peak heights.

Based on peak prominence and peak width in the existing DAS graph, we propose several feature values that can be obtained using (13) − (21), where Δw is the average difference in width (w) of the first peak and the next peak for all existing peaks, and (n) is the number of peaks that exist. The symbol Δp is the average difference in prominence (p)

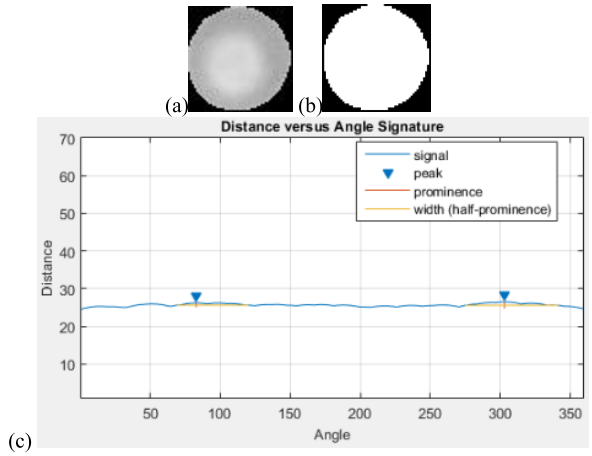

FIGURE 13. (a) Normal erythrocyte cell; (b) Binary image of normal erythrocyte cell; (c) Distance versus angle signature (DAS) graph of normal erythrocyte cell.

from all peaks. The symbol pw_{ratio} is the ratio of Δp and Δw. The symbol $\overline{p}$ is the average prominence and $\overline{w}$ is the average width. The symbol STD_{width} is the standard deviation of width and STD_{prom} is the standard deviation of prominence. The symbol $\overline{d}$ is the average distance obtained from angles $\theta = 1°$ to $\theta = 360°$. The symbol $\overline{pks}$ is the average local maxima (pks). We will use these features as a shape representation of the erythrocyte cell body. We also use them to represent the central pallor shape in erythrocytes because there are abnormal erythrocytes that can be differentiated based on their central pallor shape.

$$\Delta w = \frac{1}{n-1}\sum_{k=1}^{n}|w_k - w_{k+1,\ldots,n}| \tag{13}$$

$$\Delta p = \frac{1}{n-1}\sum_{k=1}^{n}|p_k - p_{k+1,\ldots,n}| \tag{14}$$

$$pw_{ratio} = \frac{\Delta p}{\Delta w} \tag{15}$$

$$\overline{p} = \frac{1}{n}\sum_{k=1}^{n} p_k \tag{16}$$

$$\overline{w} = \frac{1}{n}\sum_{k=1}^{n} w_k \tag{17}$$

$$STD_{width} = \sqrt{\frac{1}{n-1}\sum_{k=1}^{n}|w_k - \overline{w}|^2} \tag{18}$$

$$STD_{prom} = \sqrt{\frac{1}{n-1}\sum_{k=1}^{n}|p_k - \overline{p}|^2} \tag{19}$$

$$\overline{d} = \frac{1}{\theta-1}\sum_{k=1}^{n} d_k \tag{20}$$

$$\overline{pks} = \frac{1}{n}\sum_{k=1}^{n} pks_k \tag{21}$$

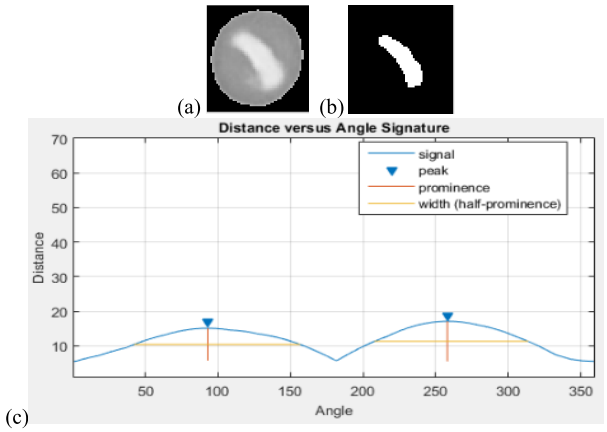

FIGURE 14. (a) Stomatocyte cell, (b) Central pallor of stomatocyte cell, (c) Distance versus angle signature (DAS) graph of stomatocyte cell central pallor.

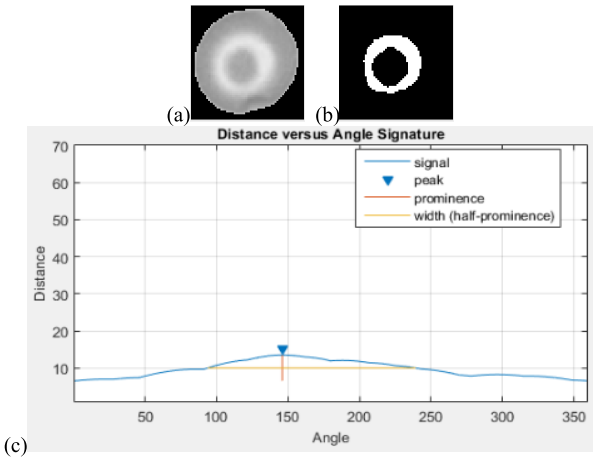

FIGURE 15. (a) Target cell, (b) Central pallor of target cell, (c) Distance versus angle signature (DAS) graph of target cell central pallor.

5) SHAPE FEATURE EXTRACTION OF CENTRAL PALLOR (CP)

The central pallor shape in circular cells is a characteristic that can be seen in abnormal erythrocytes. As shown in Fig. 5(e) - 5(i), circular erythrocytes have different central pallor shapes. Therefore, it is essential to extract the central pallor feature as additional information for classification. The central pallor can be segmented from the entire cell using binarization, labeling, and erosion. The grayscale erythrocyte image is converted to a binary image using the Otsu method and the object is labeled. The largest object is selected and the erosion operation is performed on it. The largest object after erosion is chosen as the central pallor. If there is no object after erosion, the cell has no central pallor. The features extracted from the central pallor are geometry parameters, namely area, perimeter, major axis, minor axis, compactness, eccentricity, solidity, and CP ratio (comparison of the central area to the cell area). We also extracted the DAS morphological features of the central pallor based on (13) − (21). DAS graph samples of the central pallor are shown in Figs. 14 and 15.

D. CLASSIFICATION

The classification stage in this study has been performed using machine learning algorithms, namely multilayer perceptron (MLP) with backpropagation learning methods. The backpropagation training method is widely used because the training process is relatively fast and provides relatively good accuracy. We used the MLP based on preliminary studies that were conducted to classify erythrocytes [19], [27]. This study used two datasets. The D1 dataset contains 7108 single erythrocyte sub-images obtained from the results of cell segmentation. The D2 dataset consists of 2247 single erythrocyte sub-images that are a subset of the D1 dataset. The D2 dataset was produced based on threshold criteria in Elsalamony's research [9]. Both datasets consist of nine types of erythrocytes. The first experiment used the D1 dataset to determine the effect of the selected features on classification performance. The second experiment used the D2 dataset to compare the classification performance of the proposed method with the previous work [9].

The MLP parameters used in this study were obtained based on the best experimental results using various levels of the learning rate, momentum, and epoch. In the experiment, we used combination values of 0.01, 0.05, and 0.10 for learning rate, the values of 0.2, 0.4, 0.6, and 0.8 for momentum, and the values of 1000, 5000, and 10000 for the number of epochs. The number of hidden layer nodes was obtained using (22) based on Huang [28], where L_1 is the number of hidden layer nodes, m is the number of classes, and N is the number of inputs.

$$L_1 = \sqrt{(m+2)N} + 2\sqrt{N/(m+2)} \tag{22}$$

Input for MLP is the feature value of the feature extraction. In the first experiment, we used a k-fold cross-validation method to avoid overfitting, with a value of k = 10. In this process, input data was divided into ten parts; nine parts were used as training data, and one part as testing data. Each testing process will use approximately 10% of the total data, which is 6398 images as training data and 710 images as testing data. The training and testing process will be performed ten times until all data has been used as training data and testing data. In the next stage, the performance of the classification model is evaluated using a confusion matrix that shows the relationship between the predicted class and the actual class. The second experiment aims to compare the classification results using the features in the proposed method with the classification results using features proposed in the previous work [9].

E. PERFORMANCE MEASURES

The parameters used to measure the success of classification in this study were accuracy, sensitivity, specificity, and receiver operating characteristic curve (ROC). Measurement of model performance accuracy was chosen to determine the ability of the model to detect all objects correctly. Sensitivity

TABLE 2. Classification performance with combination of features.

	No	Features	Number of features	Accuracy (%)	Average Specificity (%)	Average Sensitivity (%)	ROC Area
Texture	1	GLCM	20	84.99	98.03	69.06	0.90
Texture + color	2	GLCM + color moment	24	89.32	98.60	74.74	0.93
Shape	3	Moment invariants + geometry parameters of cell	14	78.21	97.11	55.30	0.89
	4	DAS morphology of cell and central pallor	18	90.39	98.79	74.96	0.91
	5	Geometry parameters of cell and central pallor	15	94.15	99.25	81.47	0.97
	6	Moment invariants + geometry parameters of cell and central pallor	22	94.18	99.26	81.57	0.99
	7	Moment invariants + geometry parameters of cell and central pallor + DAS morphology of cell and central pallor	40	95.05	99.37	82.58	0.98
	8	Geometry parameters of cell and central pallor + DAS morphology of cell and central pallor	33	95.23	99.40	92.69	0.99
Texture + color + shape	9	GLCM + color moment + moment invariants + geometry parameters of cell	38	92.81	99.08	78.96	0.97
	10	GLCM + color moment + moment invariants + geometry parameters of cell and central pallor	46	97.73	99.71	86.17	0.98
	11	GLCM + color moment + geometry parameters of cell and central pallor	39	97.33	99.65	85.50	0.98
	12	GLCM + color moment + DAS morphology of cell + DAS morphology of central pallor	42	95.50	99.43	83.01	0.99
	13	All-features: GLCM + color moment + moment invariants + geometry parameters of cell and central pallor + DAS morphology of cell and central pallor	64	98.11	99.75	86.67	0.99

and specificity were chosen because a diagnostic test for screening must have very high sensitivity even if the specificity is slightly low [29]. ROC is commonly used in medical decision making because medical data usually contains imbalanced class data. Unlike measures that depend on the accuracy of the majority class, the ROC is not affected by the majority class. ROC is a trade-off between the sensitivity (TP rate) and FP rate values, and is used to measure the accuracy of the model. Equations used to calculate accuracy, sensitivity, and specificity are shown in (23) − (25).

$$Accuracy = \frac{TP + TN}{TP + TN + FP + FN} \tag{23}$$

$$Sensitivity = \frac{TP}{TP + FN} \tag{24}$$

$$Spesificity = \frac{TN}{TN + FP} \tag{25}$$

IV. RESULT AND DISCUSSION

This section presents an evaluation of erythrocyte cell classification performance. The comparison result of erythrocyte classification based on the selected features is shown in Table 2. According to the global performance measure in Table 2, it can be observed that combining feature types produces higher accuracy than using only one type of feature. GLCM features can achieve 84.99% accuracy. When we combine GLCM features with color moments, accuracy improves to 89.32%. The morphological features produce higher accuracy than texture and color features. The combination of moment invariants and the geometry parameters of the cell yields an accuracy of 78.21%, whereas the DAS morphological features of the cell and central pallor (CP) yield an accuracy of 90.39%. When we combine the geometry parameters of the cell and CP, we achieve an accuracy of 94.15%. However, when we use the combination of moment invariants, geometry parameters of the cell and CP, we reach an accuracy of 94.18%. Furthermore, combining the geometry parameters of the cell and CP with DAS morphological features of the cell and CP yielded an accuracy of 95.23%. Comparing morphological features, combination of the geometry parameters of the cell and CP with DAS morphological features of the cell and CP achieve good accuracy for erythrocyte classification.

TABLE 3. Erythrocyte classification performance of previous work and the proposed method.

Type of cells	Sensitivity (%)		Specificity (%)	
	Elsalamony [9]	Proposed method	Elsalamony [9]	Proposed method
Elliptocytosis	93.67	98.10	99.43	99.57
Pencil cell	90.91	0.00	100.00	100.00
Teardrop cell	97.34	100.00	99.45	99.78
Normal cell	82.51	91.75	78.42	98.16
Stomatocyte	15.08	88.94	99.51	99.12
Target cell	30.28	88.38	96.13	98.73
Hypochromic	64.78	94.97	98.23	99.52
Spherocyte	69.00	94.83	94.79	98.12
Acanthocyte	98.38	97.84	99.08	99.71
Average of all classes	71.33	83.86	96.12	99.14
Accuracy of Elsalamony [9] (%)		71.56		
Accuracy of Proposed method (%)		93.77		

ERYTHROCYTE CLASSES		OUTPUT CLASS									Total
		EL	P	TD	N	ST	T	H	SP	A	
TARGET CLASS	Elliptocytosis (EL)	1206	0	0	2	2	1	0	0	0	1211
	Pencil cell (P)	15	0	8	0	0	0	0	0	1	24
	Teardrop cell (TD)	3	0	2073	0	0	0	0	0	0	2076
	Normal cell (N)	0	0	0	1402	3	11	3	5	2	1426
	Stomatocyte (ST)	3	0	2	15	356	3	0	1	2	382
	Target cell (T)	0	0	1	9	6	820	7	3	5	851
	Hypochromic (H)	1	0	0	3	0	8	210	0	0	222
	Spherocyte (SP)	0	0	0	3	0	2	0	556	1	562
	Acanthocyte (A)	0	0	0	2	0	0	1	0	351	354
	Total	1228	0	2084	1436	367	845	221	565	362	6974

FIGURE 16. Confusion matrix of proposed method for all features in dataset D1.

ERYTHROCYTE CLASSES		OUTPUT CLASS									Total
		EL	P	TD	N	ST	T	H	SP	A	
TARGET CLASS	Elliptocytosis (EL)	155	0	2	0	0	0	0	0	1	158
	Pencil cell (P)	9	0	2	0	0	0	0	0	0	11
	Teardrop cell (TD)	0	0	413	0	0	0	0	0	0	413
	Normal cell (N)	0	0	0	467	7	13	3	18	1	509
	Stomatocyte (ST)	0	0	0	10	177	4	0	8	0	199
	Target cell (T)	0	0	0	11	7	251	5	10	0	284
	Hypochromic (H)	0	0	0	1	0	4	151	0	3	159
	Spherocyte (SP)	0	0	0	9	3	4	0	312	1	329
	Acanthocyte (A)	0	0	0	1	1	0	2	0	181	185
	Total	164	0	417	499	195	276	161	348	187	2107

FIGURE 17. Confusion matrix of proposed method for all features in dataset D2.

The combination of texture, color, and shape features has been compared to show the reliability of the proposed features. The combination of GLCM features, color moments, moment invariants, and the geometry parameters of the cell yields an accuracy of 92.81%. The combination of GLCM features, color moments, and DAS morphological features of

ERYTHROCYTE CLASSES		OUTPUT CLASS									Total
		EL	P	TD	N	ST	T	H	SP	A	
TARGET CLASS	Elliptocytosis (EL)	148	0	10	0	0	0	0	0	0	158
	Pencil cell (P)	1	10	0	0	0	0	0	0	0	11
	Teardrop cell (TD)	11	0	402	0	0	0	0	0	0	413
	Normal cell (N)	0	0	0	420	3	44	0	40	2	509
	Stomatocyte (ST)	0	0	0	90	30	12	34	27	6	199
	Target cell (T)	0	0	0	161	0	86	0	33	4	284
	Hypochromic (H)	0	0	0	31	7	11	103	0	7	159
	Spherocyte (SP)	0	0	0	93	0	9	0	227	0	329
	Acanthocyte (A)	0	0	0	0	0	0	3	0	182	185
	Total	160	10	412	795	40	162	140	327	201	1608

FIGURE 18. Confusion matrix of Elsalamony method [9] in dataset D2.

the cell and CP yields an accuracy of 95.50%. Adding the geometry parameters of CP to the combination of GLCM features, color moments, moment invariants, and the geometry parameters of the cell, we produce an accuracy improvement of 4.92%. The combination of GLCM features, color moments, the geometry parameters of cell, and CP yields an accuracy of 97.33%. In addition, accuracy increased to 98.11% when all features were used. Thus, the additional features contain important information that contributes to improvement of classification accuracy. The confusion matrix of classification results using all features in dataset D1 is shown in Fig. 16.

The second experiment compared the performance of the classification results from the proposed method with previous studies that used distance angle signature features [9]. We applied the method of [9] in our primary data to produce the D2 datasets. Comparison results of classification performance are shown in Table 3. Based on the D2 dataset, the previous method [9] is superior in classifying oval-shaped cells such as elliptocytosis, pencil cells, and teardrop cells. In contrast, the proposed method is superior in classifying circular-shaped cells. In previous research [9], circular cells were considered as normal cells. In this study, we have

succeeded in classifying circular cells according to their type, as shown in sensitivity values that exceed 88.38% for normal cells, stomatocytes, target cells, hypochromic cells, spherocytes, and acanthocytes. In the previous research method [9], stomatocytes, target cells, hypochromic cells, and spherocytes were detected with sensitivity ranging from 15.08%–69.00%, whereas our study obtains higher sensitivity of 88.38%–94.97%. The accuracy of the proposed method is 93.77%, whereas the accuracy of the previous method [9] is 71.56%. The confusion matrix of the proposed method using all features in dataset D2 is shown in Fig. 17. The confusion matrix of the Elsalamony method is shown in Fig. 18.

V. CONCLUSION

This research aims to identify features that can be used to distinguish nine types of erythrocytes. Based on the results of this study, we can conclude that using one feature type does not produce maximum accuracy; using multiple feature types yields increased accuracy. The maximum accuracy obtained in this study is 98.11%, maximum specificity is 99.75%, sensitivity is 86.67%, and ROC area 0.99, based on a combination of texture, color, and morphological features. All characteristics combined include GLCM, color moment, moment invariants, geometry parameters of the cell and central pallor, DAS morphology of the cell, and DAS morphology of central pallor.

The results of the proposed method compared with previous studies show that the combined features of shape, texture, and color can be used to properly classify cells with a circular shape. The classification accuracy is increased for all nine cell types. The proposed method reaches 93.77% accuracy, an increase of 22.21% from previous studies. For future work, feature selection will be modified to achieve high accuracy with a smaller number of features.

ACKNOWLEDGMENT

The authors would like to thank the Clinical Pathology Laboratory, the Faculty of Medicine, Public Health and Nursing, Universitas Gadjah Mada, for providing data for this research. They also thank the Research Directorate of Universitas Gadjah Mada in the Rekognisi Tugas Akhir 2019 scheme and also thank the Indonesian Ministry of Research, Technology and Higher Education, in PMDSU scheme for funding this research.

REFERENCES

[1] A. Akay, A. Dragomir, A. Yardimci, D. Canatan, A. Yesilipek, and B. W. Pogue, "A data-mining approach for investigating social and economic geographical dynamics of β-Thalassemia's spread," *IEEE Trans. Inf. Technol. Biomed.*, vol. 13, no. 5, pp. 774–780, Sep. 2009.

[2] M. Marinelli, B. Gianesin, M. Balocco, P. Beruto, C. Bruzzone, P. Carrara, P. Gallusi, A. Macco, M. Musso, E. Oliveri, S. Pelucchi, G. Sobrero, R. Villa, and G. L. Forni, "Total iron-overload measurement in the human liver region by the magnetic iron detector," *IEEE Trans. Biomed. Eng.*, vol. 57, no. 9, pp. 2295–2303, Sep. 2010.

[3] A. Farruggia, L. Agnello, P. Toia, E. Murmura, M. Russo, E. Grassedonio, M. Midiri, and S. Vitabile, "A novel expert system for non-invasive liver iron overload estimation in thalassemic patients," in *Proc. 8th Int. Conf. Complex, Intell. Softw. Intensive Syst.*, Jul. 2014, pp. 107–112.

[4] L. Palmer, C. Briggs, S. McFadden, G. Zini, J. Burthem, G. Rozenberg, M. Proytcheva, and S. J. Machin, "ICSH recommendations for the standardization of nomenclature and grading of peripheral blood cell morphological features," *Int. J. Lab. Hematol.*, vol. 37, no. 3, pp. 287–303, Jun. 2015.

[5] R. Tomari, W. N. W. Zakaria, M. M. A. Jamil, F. M. Nor, and N. F. N. Fuad, "Computer aided system for red blood cell classification in blood smear image," *Procedia Comput. Sci.*, vol. 42, pp. 206–213, Jan. 2014.

[6] O. Sarrafzadeh, A. M. Dehnavi, H. Rabbani, N. Ghane, and A. Talebi, "Circlet based framework for red blood cells segmentation and counting," in *Proc. IEEE Workshop Signal Process. Syst. (SiPS)*, Oct. 2015, pp. 1–6.

[7] H. Chauris, I. Karoui, P. Garreau, H. Wackernagel, P. Craneguy, and L. Bertino, "The circlet transform: A robust tool for detecting features with circular shapes," *Comput. Geosci.*, vol. 37, no. 3, pp. 331–342, Mar. 2011.

[8] M. Gonzalez-Hidalgo, F. A. Guerrero-Pena, S. Herold-Garcia, A. Jaume-I-Capo, and P. D. Marrero-Fernandez, "Red blood cell cluster separation from digital images for use in sickle cell disease," *IEEE J. Biomed. Health Informat.*, vol. 19, no. 4, pp. 1514–1525, Jul. 2015.

[9] H. A. Elsalamony, "Anaemia cells detection based on shape signature using neural networks," *Measurement*, vol. 104, pp. 50–59, Jul. 2017.

[10] S. Hartati, A. Harjoko, R. Rosnelly, I. Chandradewi, and Faizah, "Performance of SVM and ANFIS for classification of malaria parasite and its life-cycle-stages in blood smear," *Commun. Comput. Inf. Sci.*, vol. 937, 2018, pp. 110–121.

[11] A. Setiawan, A. Harjoko, T. Ratnaningsih, E. Suryani, Wiharto, and S. Palgunadi, "Classification of cell types in acute myeloid leukemia (AML) of M4, M5 and M7 subtypes with support vector machine classifier," in *Proc. Int. Conf. Inf. Commun. Technol. (ICOIACT)*, Mar. 2018, pp. 45–49.

[12] J. Rodellar, S. Alférez, A. Acevedo, A. Molina, and A. Merino, "Image processing and machine learning in the morphological analysis of blood cells," *Int. J. Lab. Hematol.*, vol. 40, pp. 46–53, May 2018.

[13] M. Z. Othman, T. S. Mohammed, and A. B. Ali, "Neural network classification of white blood cell using microscopic images," *Int. J. Adv. Comput. Sci. Appl.*, vol. 8, no. 5, pp. 99–104, 2017.

[14] S. N. Mohd Safuan, M. R. Md Tomari, and W. N. Wan Zakaria, "White blood cell (WBC) counting analysis in blood smear images using various color segmentation methods," *Measurement*, vol. 116, pp. 543–555, Feb. 2018.

[15] M. Tyagi, L. M. Saini, and N. Dahyia, "Detection of poikilocyte cells in iron deficiency anaemia using artificial neural network," in *Proc. Int. Conf. Comput. Power, Energy Inf. Commun. (ICCPEIC)*, Apr. 2016, pp. 108–112.

[16] P. T. Dalvi and N. Vernekar, "Computer aided detection of abnormal red blood cells," in *Proc. IEEE Int. Conf. Recent Trends Electron., Inf. Commun. Technol. (RTEICT)*, May 2016, pp. 1741–1746.

[17] Z. M. Abood, G. S. Karam, and R. E. Hluot, "Classification of red blood cells disease using fuzzy logic theory," in *Proc. Int. Conf. Current Res. Comput. Sci. Inf. Technol. (ICCIT)*, Apr. 2017, pp. 31–36.

[18] I. Ahmad, S. Norul, and R. Zahratul, "Morphological features analysis for erythrocyte classification in IDA and thalassemia," *Int. J. Adv. Comput. Sci. Appl.*, vol. 9, no. 12, pp. 274–280, 2018.

[19] D. A. Tyas, T. Ratnaningsih, A. Harjoko, and S. Hartati, "The classification of abnormal red blood cell on the minor thalassemia case using artificial neural network and convolutional neural network," in *Proc. Int. Conf. Video Image Process. (ICVIP)*, 2017, pp. 228–233.

[20] V. Sharma, A. Rathore, and G. Vyas, "Detection of sickle cell anaemia and thalassaemia causing abnormalities in thin smear of human blood sample using image processing," in *Proc. Int. Conf. Inventive Comput. Technol. (ICICT)*, vol. 3, Aug. 2016, pp. 1–5.

[21] H. A. Aliyu, R. Sudirman, M. A. A. Razak, and M. A. A. Wahab, "Red blood cells abnormality classification: Deep learning architecture versus support vector machine," *Int. J. Integr. Eng.*, vol. 10, no. 7, pp. 34–42, Nov. 2018.

[22] F. Qin, N. Gao, Y. Peng, Z. Wu, S. Shen, and A. Grudtsin, "Fine-grained leukocyte classification with deep residual learning for microscopic images," *Comput. Methods Programs Biomed.*, vol. 162, pp. 243–252, Aug. 2018.

[23] R. M. Haralick, K. Shanmugam, and I. Dinstein, "Textural features for image classification," *IEEE Trans. Syst., Man, Cybern.*, vol. SMC-3, no. 6, pp. 610–621, Nov. 1973.

[24] T. Acharya and A. K. Ray, *Image Processing: Principle and Applications*. Hoboken, NJ, USA: Wiley, 2005.

[25] M.-K. Hu, "Visual pattern recognition by moment invariants," *IEEE Trans. Inf. Theory*, vol. 8, no. 2, pp. 179–187, Feb. 1962.
[26] R. C. Gonzalez and R. E. Woods, *Digital Image Processing*, 3rd ed. Upper Saddle River, NJ, USA: Prentice-Hall, 2008.
[27] D. A. Tyas, S. Hartati, A. Harjoko, and T. Ratnaningsih, "Erythrocyte classification using multi-layer Perceptron, Naïve Bayes classifier, RBF network and SVM," *Int. J. Eng. Advance Technol.*, vol. 9, no. 2, pp. 2024–2028, 2019.
[28] G.-B. Huang, "Learning capability and storage capacity of two-hidden-layer feedforward networks," *IEEE Trans. Neural Netw.*, vol. 14, no. 2, pp. 274–281, Mar. 2003.
[29] S. Sastroasmoro and S. Ismael, *Fundamentals of Clinical Research Methods (Dasar-dasar Metodologi Penelitian Klinis)*, 4th ed. Jakarta, Indonesia: CV. Sagung Seto, 2011.

DYAH ARUMING TYAS received the bachelor's degree in electronics and instrumentation from Universitas Gadjah Mada (UGM), Yogyakarta, Indonesia, in 2013, where she is currently pursuing the Ph.D. degree with the Department of Computer Science and Electronics. Her research interests include image processing and artificial intelligence.

SRI HARTATI received the bachelor's degree in electronics and instrumentation from Universitas Gadjah Mada (UGM), Yogyakarta, Indonesia, in 1986, and the M.Sc. and Ph.D. degrees in computer science from the University of New Brunswick, Fredericton, NB, Canada, in 1990 and 1996, respectively. She is currently a Professor and a member of the Intelligent System Laboratory, Department of Computer Science and Instrumentation, UGM, Yogyakarta, Indonesia. Her research interests include artificial and computational intelligence, and decision support systems.

AGUS HARJOKO received the bachelor's degree in electronics and instrumentation from Universitas Gadjah Mada (UGM), Yogyakarta, Indonesia, in 1986, and the M.Sc. and Ph.D. degrees in computer science from the University of New Brunswick, Fredericton, NB, Canada, in 1990 and 1996, respectively. He is currently an Associate Professor and the Head of the Department of Computer Science and Instrumentation, UGM. His research interests include computer vision, pattern recognition, instrumentation, and sensor networks.

TRI RATNANINGSIH received the Medical Doctor degree from the Faculty of Medicine, Gadjah Mada University, Indonesia, in 1995, and the master's degree in tropical medical science and the Ph.D. degree in health science from Gadjah Mada University. Subsequently, she continued her career as a Clinical Pathologist and became a Hematology and Transfusion Medicine consultant, in 2014. She is currently a Lecturer and holds the position of Head of the Department of Clinical Pathology and the Laboratory Medicine, Universitas Gadjah Mada, Indonesia.